Spectral properties of entangled photons generated via type-I frequency-nondegenerate spontaneous parametric down-conversion

So-Young Baek* and Yoon-Ho Kim†
Department of Physics, Pohang University of Science and Technology (POSTECH), Pohang 790-784, Korea
(Received 7 April 2009; published 9 September 2009)

Spectral properties of entangled photons generated via type-I frequency-nondegenerate spontaneous parametric down-conversion are studied theoretically and experimentally. For monochromatic pumping, the joint spectral intensity function for the photon pair is found to be symmetric even though each photon has a different central wavelength. The single-photon (first-order) interference shows the familiar triangular interferogram, usually associated with the cw-pumped frequency-degenerate type-II spontaneous parametric down-conversion. For broadband (ultrafast) pumping, on the other hand, the joint spectral intensity function is shown to be asymmetric, similar to the case of ultrafast-pumped frequency-degenerate type-II spontaneous parametric down-conversion. The spectral studies reported here are expected to play an important role in developing ultrabright two-color entangled photon sources.

DOI: 10.1103/PhysRevA.80.033814 PACS number(s): 42.65.Lm, 03.67.Mn, 03.65.Wj, 42.50.Dv

I. INTRODUCTION

The spontaneous parametric down-conversion (SPDC), a second-order nonlinear optical process in which a higher-energy pump photon is split into a pair of lower-energy daughter photons inside the nonlinear crystal [1], has played important roles in the recent progress of experimental quantum optics and quantum information. The SPDC process was initially used for studying nonclassical properties of light [2–6] and foundational problems in quantum physics [7–9]. In the recent years, the SPDC process is essential in experimental quantum information as the most practical and efficient source of entanglement in polarization [7,10–16], in energy-time [17–22], in position-momentum [23–27], in photon-number–path [3,28,29], and in other variables [30–38].

The physical properties of SPDC radiation is determined by the phase matching condition which is characterized with the polarization, frequencies, and the propagation directions of the interacting photons. Of particular importance is the single- and joint-spectral properties of SPDC photons not only because they determine the amount of inherent entanglement between the SPDC photons [39–41] but also because entanglement in other photonic degrees of freedom is significantly affected by the spectral properties of SPDC.

For type-II SPDC, in which the down-converted photons have orthogonal polarization, the spectral properties are now well studied both by frequency-selective detection [42–44] and by interferometric detection [45–48] of the SPDC photons. For type-I SPDC, the down-converted photons are identically polarized and this in general requires the phase matching function to be treated differently from the case of type-II SPDC, resulting in different spectral properties [48]. In particular, frequency-degenerate type-I SPDC exhibits the differences most clearly and we have recently reported detailed experimental and numerical studies on spectral properties of frequency-degenerate type-I SPDC photons [49]. Note that frequency-degenerate SPDC leads to two photons that have the same central frequencies but with negative frequency correlation between the photon pair [43,49]. It is also worth reminding that the quantum state of the photon pair should be described as a coherent quantum superposition of many frequency-anticorrelated photon pair amplitudes, not as a classical mixture.

Recently, the frequency-nondegenerate SPDC, in which the two entangled photons have different central frequencies, have found to be important in implementing a wide variety of quantum information protocols, including quantum communication [14,50,51], high-dimensional quantum states [52–55], a photon-matter quantum interface [56,57], and quantum metrology [58,59]. For type-II SPDC, the frequency-nondegenerate case is expected to exhibit similar spectral properties to the frequency-degenerate case since the phase matching function is treated the same. On the other hand, for type-I SPDC, the frequency-nondegenerate case and the frequency-degenerate case are expected to exhibit different spectral (hence temporal) properties as the analytical treatment of the phase matching function must differ due to the large differences in the group velocities of the frequency-nondegenerate SPDC photons [48]. To date, however, the spectral properties of frequency-nondegenerate type-I SPDC have not been subjected to extensive experimental studies.

In this paper, we report experimental and theoretical studies on the spectral properties of entangled photons generated via frequency-nondegenerate type-I SPDC for both cw- and ultrafast-pumping configurations. The joint spectral properties are investigated by experimentally mapping the two-photon spectral intensity function and the single-photon spectra are studied by observing the first-order interference with a Michelson interferometer. The spectral properties of frequency-nondegenerate type-I SPDC will then be compared with those of type-II SPDC [43,44,60] and frequency-degenerate type-I SPDC [45,48,49].

*simply@postech.ac.kr
†yoonho@postech.ac.kr

II. SPECTRAL PROPERTIES OF TYPE-I SPDC

For the SPDC process to occur in a noncentrosymmetric crystal, the photons involved in the SPDC process should satisfy the phase matching condition, $\vec{k}_1+\vec{k}_2=\vec{k}_p$, and $\omega_1+\omega_2=\omega_p$. Here, $\vec{k}_p$ and ω_p refer to the momentum and the frequency of the pump photon. Since the phase matching is not perfect due to the material dispersion and the finite thickness of the nonlinear crystal, the phase mismatch function $\vec{\Delta}=\vec{k}_p-\vec{k}_1-\vec{k}_2$ is nonzero.

Assuming that the pump photon propagates in the z direction and is not tightly focused, the transverse (in the x-y plane) phase matching can be regarded to be perfect, $\vec{\Delta}_\perp=\vec{k}_{1\perp}+\vec{k}_{2\perp}\approx 0$, and this condition gives rise to a strong transverse quantum correlation between two SPDC photons [58]. However, the longitudinal phase mismatch, $\Delta_z=k_p-k_{1z}-k_{2z}$, cannot be ignored and it is, in fact, the longitudinal phase mismatch that mainly affects the spectral properties of SPDC photons.

The longitudinal phase mismatch Δ_z in type-I SPDC can be calculated to be [49],

$$\Delta_z(\lambda_1,\lambda_2,\theta_1^\circ)=k_p(\lambda_p,\Psi)-k_1(\lambda_1)\sqrt{1-\left(\frac{\sin\theta_1^\circ}{n_o(\lambda_1)}\right)^2}-k_2(\lambda_2)\sqrt{1-\left(\frac{\lambda_2}{\lambda_1}\right)^2\left(\frac{\sin\theta_1^\circ}{n_o(\lambda_2)}\right)^2}, \quad (1)$$

where $k_p(\lambda_p,\Psi)=2\pi n_{\text{eff}}(\lambda_p,\Psi)/\lambda_p$. Here, Ψ and n_{eff}, respectively, are the angle of the optic axis with respect to $\vec{k}_p$ and the effective refractive index of the pump photon. The angle θ_1° is the mean emission angle (outside the crystal) of the signal photon. The mean emission angle of the idler photon θ_2° can be calculated from θ_1° using $\vec{k}_1+\vec{k}_2=\vec{k}_p$.

The quantum state of SPDC is then written as [42]

$$|\psi\rangle=C\int\int d\omega_1 d\omega_2\ \text{sinc}\left(\frac{\Delta_z L}{2}\right)\mathcal{E}_p(\omega_1+\omega_2)a_1^\dagger(\omega_1)a_2^\dagger(\omega_2)|0\rangle, \quad (2)$$

where C is a constant, L is the crystal thickness, and Δ_z is the longitudinal phase mismatch term defined in Eq. (1). The pump envelope is assumed to be Gaussian, $\mathcal{E}_p(\omega_1+\omega_2)=\exp[-(\omega_1+\omega_2)^2/\sigma_p^2]$, where σ_p and Ω_p are the bandwidth and the central frequency, respectively, of the pump laser. Finally, $a_1^\dagger(\omega_1)$ and $a_2^\dagger(\omega_2)$ are the creation operators for the signal and the idler photons of frequencies ω_1 and ω_2, respectively.

Clearly, the spectral properties of SPDC photons are contained in the joint spectrum intensity function $\mathcal{S}(\lambda_1,\lambda_2,\theta_1^\circ)$, defined as

$$\mathcal{S}=\left|\text{sinc}\left(\frac{\Delta_z(\lambda_1,\lambda_2,\theta_1^\circ)L}{2}\right)\mathcal{E}_p\left(\frac{1}{\lambda_1}+\frac{1}{\lambda_2}\right)\right|^2. \quad (3)$$

The phase matching function $\text{sinc}^2(\Delta_z L/2)$ determines how the energy of the pump photon is distributed to the down-converted photons and the pump envelope function $\mathcal{E}_p^2(1/\lambda_1+1/\lambda_2)$ governs the strength of frequency correlation of two down-converted photons. Since the pump envelope function depends on the sum of the frequencies of the two down-converted photons, it is always symmetric with respect to the $\lambda_1=\lambda_2$ line. Thus, symmetry (or asymmetry) of the joint spectral intensity function $\mathcal{S}$ is primarily determined by the shape of the phase matching function $\text{sinc}^2(\Delta_z L/2)$.

The two-photon joint spectral intensity function as well as the single-photon spectra can then be evaluated from Eq. (3) by setting the collection angles to correspond to the conditions of the experiment, e.g., the aperture size and the locations of the irises [49]. It is convenient to rewrite the phase mismatch function [Eq. (1)] in the frequency domain as

$$\Delta_z=k_p(\omega_p)-k_1(\omega_1)c_1(\omega_1,\theta_1^\circ)-k_2(\omega_2)c_2(\omega_2,\theta_1^\circ), \quad (4)$$

where $c_1(\omega_1,\theta_1^\circ)=\sqrt{1-[\sin\theta_1^\circ/n_o(\omega_1)]^2}$ and $c_2(\omega_2,\theta_1^\circ)=\sqrt{1-[(\Omega_p-\omega_2)/\omega_2]^2[\sin\theta_1^\circ/n_o(\omega_2)]^2}$. By introducing the detuning frequency ν_i with $\omega_i=\Omega_i+\nu_i$ $(i=p,1,2)$, each term in Eq. (4) can be expanded as

$$k_p(\omega_p)\approx k_p(\Omega_p)+\nu_p k_p'(\Omega_p),$$

$$k_i(\omega_i)c_i(\omega_i,\theta_1^\circ)\approx k_i(\Omega_i)c_i(\Omega_i,\theta_1^\circ)+\nu_i\{k_i'(\Omega_i)c_i(\Omega_i,\theta_1^\circ)+k_i(\Omega_i)c_i'(\Omega_i,\theta_1^\circ)\}, \quad (5)$$

where Ω_i are the central frequencies of the down-converted photons, $k_i'(\Omega_i)\equiv dk/d\omega|_{\Omega_i}$, and $c_i'(\Omega_i,\theta_i^\circ)\equiv dc_i(\omega,\theta_i^\circ)/d\omega|_{\Omega_i}$. Since Δ_z is nonzero but very small, only leading-order terms are considered in Eq. (5). Finally, the phase mismatch function in Eq. (4) can then be evaluated as

$$\Delta_z(\nu_1,\nu_2,\theta_1^\circ)\approx \nu_1\{k_p'(\Omega_p)-k_1'(\Omega_1)c_1(\Omega_1,\theta_1^\circ)-k_1(\Omega_1)c_1'(\Omega_1,\theta_1^\circ)\}+\nu_2\{k_p'(\Omega_p)-k_2'(\Omega_2)c_2(\Omega_2,\theta_1^\circ)-k_2(\Omega_2)c_2'(\Omega_2,\theta_1^\circ)\}, \quad (6)$$

using the fact that $k_p(\Omega_p)=k_1(\Omega_1)c_1(\Omega_1,\theta_1^\circ)+k_2(\Omega_2)c_2(\Omega_2,\theta_1^\circ)$ and $\nu_p=\nu_1+\nu_2$.

The differences between the frequency-degenerate and the frequency-nondegenerate type-I SPDC can now be seen in Eq. (6). For frequency-degenerate type-I SPDC, $\Omega_1=\Omega_2$ so that the phase mismatch function satisfies the relation $\Delta(\nu_1,\nu_2,\theta_1^\circ)=\Delta(\nu_2,\nu_1,\theta_1^\circ)$, exhibiting symmetry about the $\nu_1=\nu_2$ axis. On the other hand, the phase mismatch function for frequency-nondegenerate type-I SPDC exhibits asymmetry about the $\nu_1=\nu_2$ axis due to the fact that $\Delta(\nu_1,\nu_2,\theta_1^\circ)\neq\Delta(\nu_2,\nu_1,\theta_1^\circ)$, similar to the case of type-II SPDC.

III. CW-PUMPED FREQUENCY-NONDEGENERATE TYPE-I SPDC

For cw-pumped type-I SPDC, we may assume that the pump is monochromatic, i.e., $\nu_p=0$, and thus $\nu_1=-\nu_2=\nu$. Then, the phase mismatch function in Eq. (6) simplifies to

$$\Delta_z(\nu,\theta_1^\circ)\approx \nu\{k_1'(\Omega_1)c_1(\Omega_1,\theta_1^\circ)+k_1(\Omega_1)c_1'(\Omega_1,\theta_1^\circ)-k_2'(\Omega_2)c_2(\Omega_2,\theta_1^\circ)-k_2(\Omega_2)c_2'(\Omega_2,\theta_1^\circ)\}\equiv \nu D(\Omega_1,\Omega_2,\theta_1^\circ) \quad (7)$$

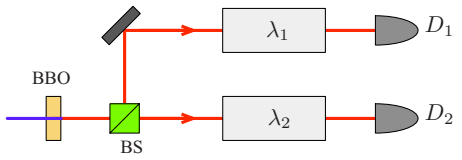

FIG. 1. (Color online) The experimental setup for measuring the joint spectral intensity function of collinear frequency-nondegenerate type-I SPDC. Two separate monochromators λ_1 and λ_2 are used for the joint spectral measurement.

and the pump envelope function $\mathcal{E}_p^2(1/\lambda_1+1/\lambda_2)$ in Eq. (3) is approximated as $\delta(\nu_1+\nu_2)$. Note that the phase mismatch function for frequency-nondegenerate type-I SPDC in Eq. (7) is proportional to the first-order of the detuning frequency ν, just as in the case of type-II SPDC [42,43]. On the other hand, for frequency-degenerate type-I SPDC, the phase mismatch function involves ν^2 terms as the first-order terms cancel out [49]. As a result, frequency-degenerate type-I SPDC exhibits a very broad spectral width, much broader than frequency-nondegenerate type-I SPDC.

The joint spectral intensity function for cw-pumped frequency-nondegenerate type-I SPDC is, therefore, found to be

$$S(\nu) = \mathrm{sinc}^2\left(\frac{\nu D(\Omega_1,\Omega_2,\theta_1^\circ)L}{2}\right), \tag{8}$$

and the complete spectral information about the SPDC photons can be found by investigating Eq. (8). It is interesting to observe that, while the phase mismatch function in Eq. (6) is in general asymmetric, when the pump is monochromatic, the two-photon joint spectral intensity function for frequency-nondegenerate type-I SPDC becomes symmetric in ν, similar to the case of cw-pumped type-II SPDC [42,43]. We therefore expect from Eq. (8) that the spectral properties of frequency-nondegenerate type-I SPDC would be similar to those of type-II SPDC, rather than those of type-I SPDC.

To conduct an experimental investigation of the two-photon joint spectral intensity function of frequency-nondegenerate type-I SPDC, we employed the frequency-resolved coincidence detection method (see Fig. 1) [43,49]. First, a type-I β-barium borate (BBO) crystal pumped by a cw argon laser operating at 351.1 nm generates a pair of entangled photons via the collinear frequency-nondegenerate type-I SPDC process. The signal and the idler photons are centered at 632.8 and 788.7 nm, respectively. A beam splitter (BS) is used to split the beam into two spatial modes.

The type-I BBO crystal was tuned for the desired frequency-nondegenerate SPDC condition by maximizing the coincidence between the two detectors D_1 and D_2 equipped with narrow-band spectral filters at 632.8 and 788.7 nm, respectively. Once the correct angle of the BBO crystal has been set, the narrow-band filters were removed and monochromators λ_1 and λ_2 were placed in front of each detector for the frequency-resolved coincidence detection. In this experiment, a 1/4 m monochromator (CS260 from Oriel) with a 600 grooves/mm grating (blaze wavelength at 400 nm) and a 1/2 m monochromator (DK480 from CVI) with a 1200 grooves/mm grating blazed at 750 nm were used. They are, respectively, labeled as λ_1 and λ_2 in Fig. 1. To focus and collimate the photons into and out of the monochromators λ_1 and λ_2, a set of lenses with $f=25$ mm and $f=50$ mm were used,
respectively.

Figure 2 shows the calculated two-photon joint spectral intensity function using Eq. (8) and the experimentally observed one. For the calculated two-photon joint spectral intensity function shown in Fig. 2(a), we assumed the collection angles for the SPDC photons to be 0.1° and the bandwidth [at full width at half maximum (FWHM)] of the pump laser to be 0.1 nm. The experimental data shown in Fig. 2(b) agree well with the numerically calculated one. The background shown in the experimental data is due to the accidental coincidences.

It is interesting to note that the joint spectral intensity functions shown in Figs. 2(a) and 2(b) appear to be asymmetric even though Eq. (8) predicts a symmetric one. The reason for this discrepancy is that Eq. (8) is expressed as a function of detuning frequency ν while the theory and the data plots in Figs. 2(a) and 2(b) are displayed in the wavelength scale as measured with the monochromators. Thus, to see how the energy of pump photon is distributed to the signal and the idler photons, it is more proper to analyze the joint spectral intensity function in detuning frequencies rather than in wavelengths. The conversion can be accomplished by using the relation between the wavelength and the frequency of a photon and by using the definition of the detuning frequency. The results of the conversion are shown in Fig. 2 in which the numerical and the experimental joint spectral intensity functions are plotted in detuning frequencies ν_1 and ν_2. The numerical and the experimental joint spectral intensity plots coincide well and they are indeed symmetric in agreement with Eq. (8).

Let us now discuss the single-photon spectral properties of cw-pumped frequency-nondegenerate type-I SPDC. The single-photon spectra for the signal or the idler photon of SPDC can be evaluated, for example, by scanning λ_1 in Eq. (3) with the condition $1/\lambda_1+1/\lambda_2=1/\lambda_p$. Experimentally, this corresponds to measuring the spectral intensity of the signal or the idler photons with a grating monochromator. It is, however, difficult to accurately observe the small side lobes of sinc^2 function in Eq. (3) due to the weak nature of SPDC and low transmission efficiencies of the monochromators. In this paper, therefore, we observe the single-photon first-order interference fringes of the signal or the idler photons of SPDC and the single-photon spectral properties can be deduced from the envelope of the interference fringes.

To see how the single-photon interference fringe is related to the spectral properties, it is necessary to calculate the expected interferogram shape at an output of a Michelson interferometer. The first step in calculating the interferogram is to evaluate the reduced density matrix for the signal photon $\hat{\rho}_s$ and it is given as [47]

$$\hat{\rho}_s = \mathrm{tr}_i[\hat{\rho}] = \int_{-\infty}^{\infty} d\nu\, S(\nu) a_s^\dagger(\Omega+\nu)|0\rangle\langle 0|a_s(\Omega+\nu), \tag{9}$$

where $\hat{\rho}=|\psi\rangle\langle\psi|$. The reduced density matrix for the idler photon $\hat{\rho}_i$ can be evaluated similarly.

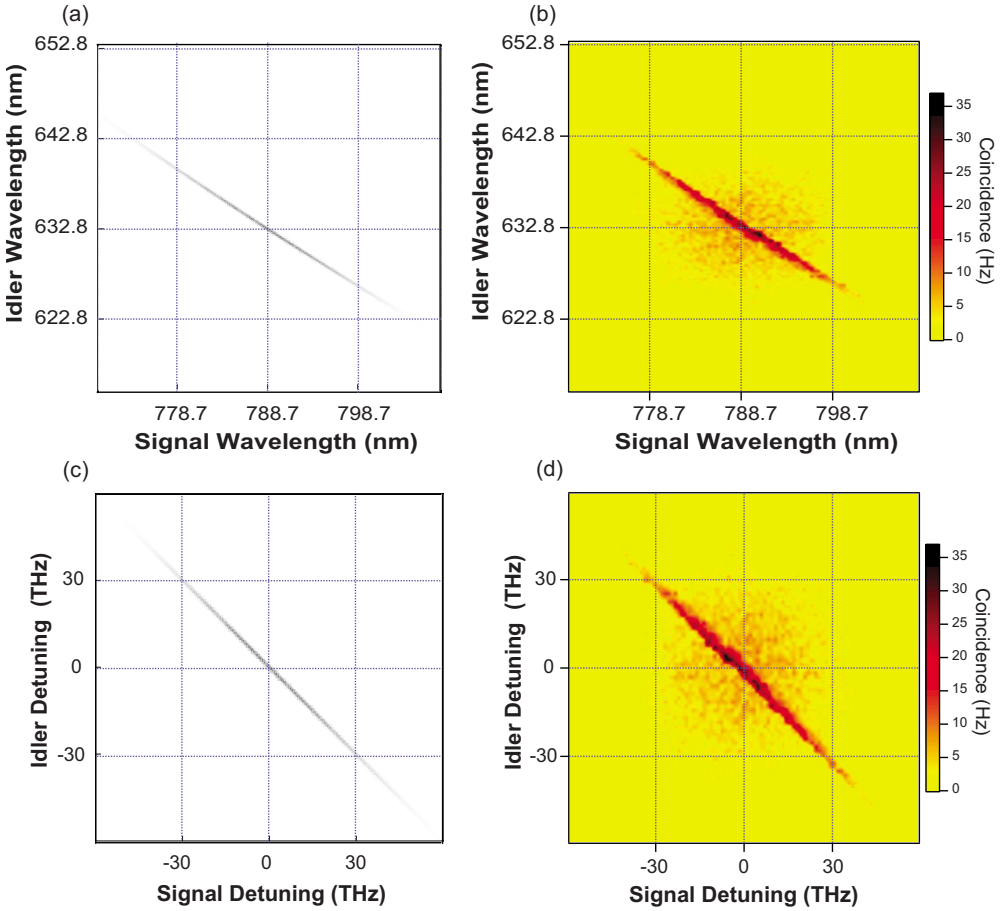

FIG. 2. (Color online) Two-photon joint spectral intensity for cw-pumped frequency-nondegenerate type-I SPDC. (a) Numerical calculation assuming the 0.1° collection angle. (b) Experimental data. The broad background (about 4 Hz in the average) results from the accidental coincidences. The joint spectral intensity function is centered at the conjugate wavelengths of 632.8 and 788.7 nm. Two-photon joint spectral intensity as a function of detuning frequencies. (c) Numerical calculation. (d) Experimental data. Note that the joint spectral intensity function for cw-pumped frequency-nondegenerate type I is symmetric about the $\nu_1=\nu_2$ axis.

The first-order correlation function of the field is then calculated to be

$$G^{(1)}(\tau)=\mathrm{tr}[\hat{\rho}_s E_s^{(-)}(t)E_s^{(+)}(t+\tau)]$$
$$=\int_0^\infty d\omega\, \mathcal{S}(\omega-\Omega)\exp(-i\omega\tau), \qquad (10)$$

where $E_s^{(-)}(t)=\int_0^\infty d\omega\, a_s^\dagger(\omega)\exp(i\omega t)$ and $\omega-\Omega=\nu$. It is clear that the first-order correlation function has a Fourier-transform relationship to the power spectrum of the signal or the idler photon.

If we now consider the experimental setup shown in Fig. 3, the normalized output R_s of the detector as a function of the Michelson interferometer delay τ is calculated to be [48]

$$R_s=tr[\hat{\rho}_s E^{(-)}(t)E^{(+)}(t)]=\tfrac{1}{2}\{1+g^{(1)}(\tau)\cos(\Omega\tau)\}, \qquad (11)$$

where $E^{(+)}(t)=\int\{a(\omega)\exp(-i\omega t)+a(\omega)\exp[-i\omega(t+\tau)]\}d\omega$ and $g^{(1)}(\tau)=|G^{(1)}(\tau)|/|G^{(1)}(0)|$. Thus, given the sinc^2 nature of the spectral property of the signal or the idler photon in Eq. (8), we expect that the single-photon interferogram for cw-pumped frequency-nondegenerate type-I SPDC measured with the experimental setup in Fig. 3 would exhibit a triangular envelope as in the case of cw-pumped type-II SPDC reported in [47,48]. Note that the triangular-shaped envelope of the single-photon interference is due to the fact that the phase mismatch function is proportional to the first order in the detuning frequency ν as shown in Eq. (8).

The experimental setup for the single-photon interference is shown in Fig. 3. To separate the SPDC photons completely from the strong pump noise, noncollinear SPDC is employed. In addition, a broadband filter was placed in front of the detector so that the actual spectral properties of the SPDC photons are not altered. First, the frequency-nondegenerate SPDC photon (the idler photon) centered at 788.7 nm, propagating at 3.5° with respect to the pump laser,

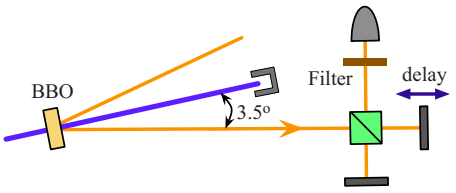

FIG. 3. (Color online) Setup for measuring the temporal coherence properties of nondegenerate type-I SPDC.

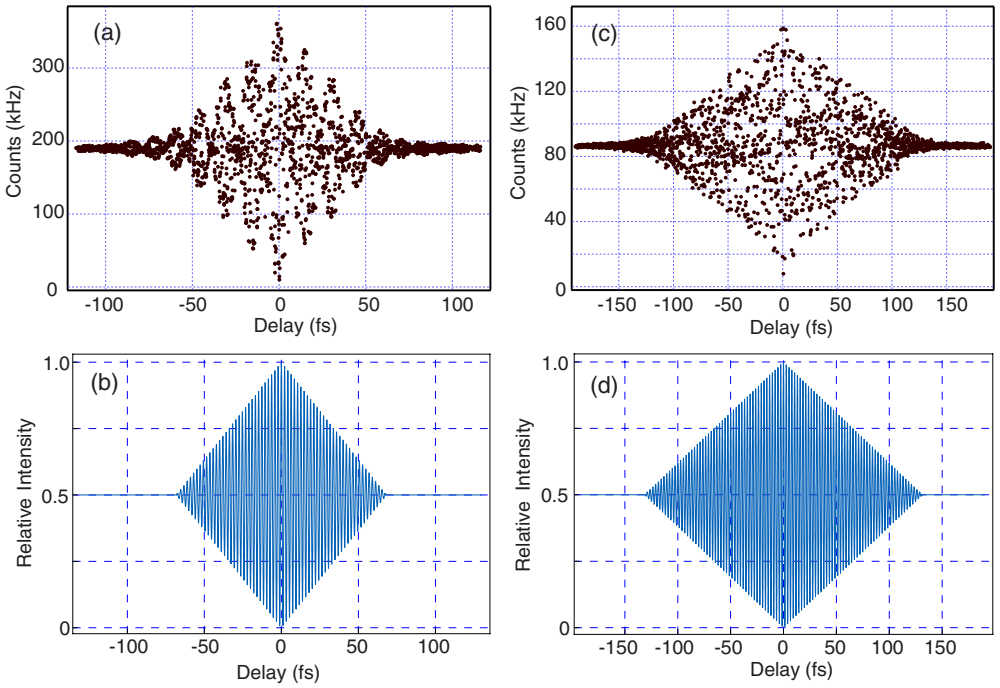

FIG. 4. (Color online) The single-photon interference patterns for cw-pumped noncollinear frequency-nondegenerate type-I SPDC. (a) The 632.8 nm centered single-photon shows a triangular shaped interference pattern and agrees well with the theoretically expected envelope shown in (b). (c) The 788.7 nm centered single-photon exhibits a similar triangular shape interference pattern, as theoretically predicted in (d).

was selected and the interference fringe pattern was recorded as a function of τ. For the 632.8 nm signal photon, the BBO crystal was slightly tilted so that the 632.8 nm signal photon would be emitted at the same 3.5° output angle.

The experimental data for the single-photon interference are shown in Fig. 4. It is evident that the frequency-nondegenerate type-I SPDC photons exhibit triangular shaped single-photon interference envelopes and the observed patters coincide well with the theoretically calculated interference fringes using Eq. (11).

Since the single-photon interferogram in Eq. (11) depends on the first-order correlation function, which is a Fourier transform of $\mathcal{S}(\nu)$ as shown in Eq. (10), the single-photon interference of the signal photon and its conjugate idler photon should show the identical width albeit with different oscillation fringes. The experimental data shown in Fig. 4, however, show different widths of the interference envelopes. This is due to the fact that the two measurements are not done for the conjugate pair photon. As mentioned above, noncollinear phase matching was chosen to suppress the pump noise and 632.8 or 788.7 nm centered photons are then selected by slightly tilting the optic axis angle. For the 632.8 nm (788.7 nm) photon propagating at 3.5° with respect to the pump, the optic axis angle for the BBO is calculated to be 33.97° (33.74°). Due to the difference in the optic axis angle, the two interference fringe patterns exhibit different widths [Figs. 4(a) and 4(c)]. The theoretically calculated interference fringes shown in Figs. 4(b) and 4(d) agree well with the experimental data and reflect the changes in the phase matching condition.

IV. ULTRAFAST-PUMPED FREQUENCY-NONDEGENERATE TYPE-I SPDC

In this section, we study the spectral properties of frequency entangled photon pairs generated via broadband- or ultrafast-pumped frequency-nondegenerate type-I SPDC. Since the joint spectral intensity function $\mathcal{S}$ in Eq. (3) is defined as the product of the phase matching function and the pump envelope function, the joint spectral intensity function of the broadband-pumped SPDC would be strongly affected by the properties of the phase mismatch function Δ_z in Eq. (6). As discussed in Sec. II, the phase mismatch function of the frequency-nondegenerate type-I SPDC in Eq. (6) is asymmetric: $\Delta(\nu_1, \nu_2, \theta_1^\circ) \neq \Delta(\nu_2, \nu_1, \theta_1^\circ)$. Thus, in the case of broadband pumping, the joint spectral intensity function for frequency-nondegenerate type-I SPDC would exhibit asymmetry, similar to the case of ultrafast-pumped frequency-degenerate type-II SPDC reported in Ref. [43].

We have measured the two-photon joint spectral intensity function for ultrafast-pumped frequency-nondegenerate type-I SPDC using the experimental setup similar to Fig. 1. A 3 mm type-I BBO crystal was pumped by frequency-doubled output of a mode-locked Ti:sapphire laser. The (frequency-doubled) pump pulse had the central wavelength of 408 nm and the FWHM bandwidth of the pulse was 3.6 nm. The pump laser was focused with a $f=500$ mm lens at the BBO crystal and the BBO crystal was setup so that frequency-nondegenerate SPDC photon pairs centered at 741 and 909 nm were propagating collinearly with the pump pulse. A beam splitter was used to split the SPDC photon pair into two spatial modes and the reflected and the trans-

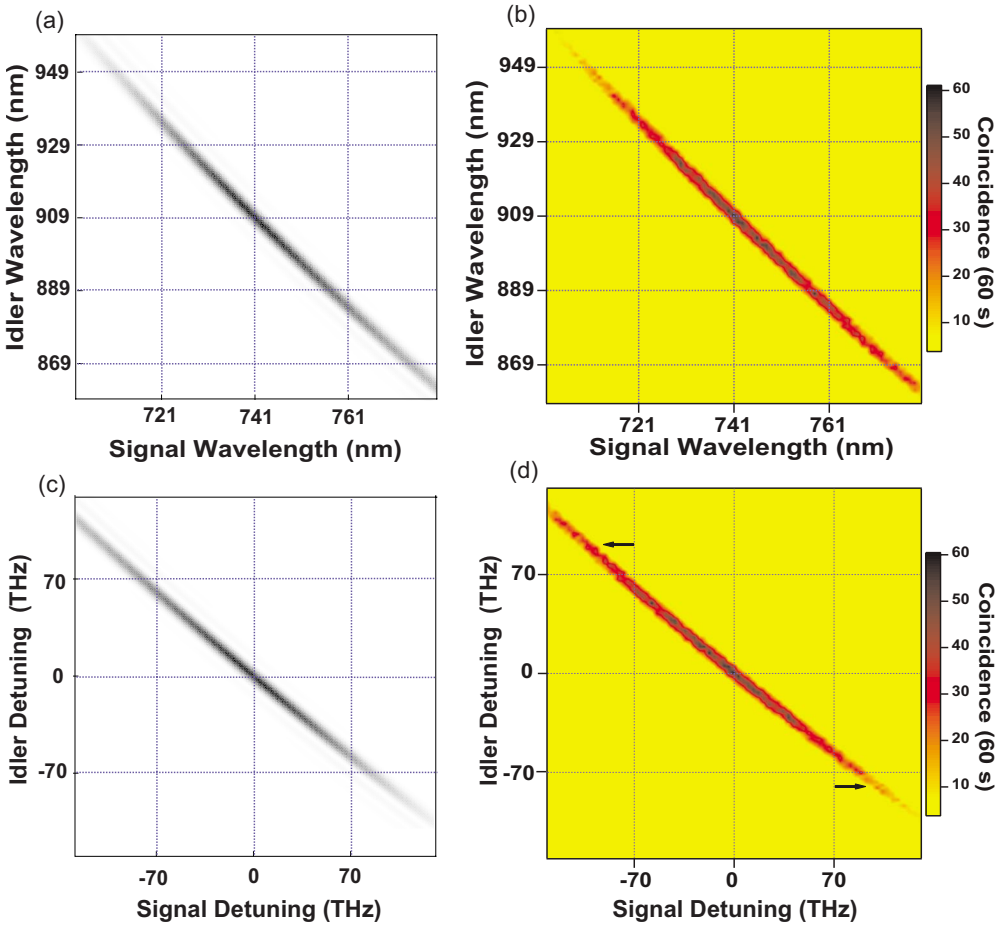

FIG. 5. (Color online) Two-photon joint spectral intensity for ultrafast-pumped frequency-nondegenerate type-I SPDC. (a) Numerical calculation assuming the 0.1° collection angle. (b) Experimental data. The joint spectral intensity function is centered at the conjugate wavelengths of 741 and 909 nm. Since we obtained the joint spectrum only for the expected data range, the broad background from the accidental coincidences is not present in this case. See the text for details. Two-photon joint spectral intensity as functions of detuning frequencies: (c) numerical calculation and (d) experimental data. Note that, differently from the cw-pumped case shown in Fig. 2, the joint spectral intensity function for ultrafast-pumped frequency-nondegenerate type-I is asymmetric about the $\nu_1=\nu_2$ axis. If the pump bandwidth is increased, the joint spectral intensity function would become more tilted in the direction of the arrows shown in (d).

mitted SPDC photons were coupled into single-mode optical fibers which were connected to the spectral measurement setup. The spectral measurement was performed with two 1/2 m monochromators (CVI DK480) with a 830/mm groove grating blazed at 1200 nm. To focus and collimate the SPDC photons into and out of the monochromators, a set of lens with $f=40$ mm was used.

The theoretically predicted and the experimentally obtained joint spectral intensity functions are shown in Fig. 5. In Fig. 5(a), the two-photon joint spectral intensity function calculated from Eq. (3) for the present experimental conditions are shown. As before, we have assumed the collection angles for the SPDC photons to be 0.1°. The experimental data shown in Fig. 5(b) fit very well with the numerically plotted results in Fig. 5(a). To save data acquisition time, we first experimentally obtained the conditional joint spectrum, by scanning monochromator λ_2 for some fixed setting values of λ_1 and then obtained the linear fitting function between the signal wavelength and the idler wavelength. Using that function we can decide the proper scanning range of λ_1 and λ_2, thus reducing the data acquisition time. As a result, the broad background from the accidental coincidences, which was shown in the cw case, is not present in the pulsed case.

To investigate how the energy of the pump photon is distributed to the SPDC photon pair, it is necessary to convert the joint spectral intensity functions [Figs. 5(a) and 5(b)] into functions of detuning frequencies ν_1 and ν_2. The results are shown in Figs. 5(c) and 5(d). The numerical simulation and the experimental data show excellent agreement and both exhibit that there exists asymmetry in the joint spectral intensity functions of ultrafast-pumped frequency-nondegenerate type-I SPDC.

V. DISCUSSION

Comparing the joint spectral intensity functions shown in Fig. 2 (cw pumped) and in Fig. 5 (ultrafast-pumped) reveals a few interesting properties. First, for broadband pumping, the SPDC photons are distributed over broader spectral ranges than the cw-pumped case. This means that, for a given frequency of the signal photon, the conjugate idler photon has a broader spectral range in broadband-pumped

case than in cw-pumped case. In other words, the degree of spectral entanglement (defined as the ratio of the single-photon spectral bandwidth to the conditional spectral bandwidth) between the photon pair is reduced as the pumping bandwidth becomes broader.

Second, while both the cw-pumped and the broadband-pumped cases exhibit frequency anticorrelation, the joint spectral intensity function for the broadband-pumped case reveals asymmetry about $\nu_1=\nu_2$. Such asymmetry is not present in the joint spectral intensity function of cw-pumped frequency-nondegenerate type-I SPDC. Furthermore, it is expected from Eqs. (3) and (6) that, as the pump bandwidth becomes broader, the asymmetry would become more pronounced in the direction of arrows in Fig. 5(d). Note that this situation is similar to the case of frequency-degenerate type-II SPDC in which ultrafast-pumping causes an asymmetric joint spectral intensity function [43]. Note also that frequency-degenerate type-I SPDC always exhibits a symmetric joint spectral intensity function regardless of the pump bandwidth [49].

VI. CONCLUSION

In this paper, we have reported experimental and theoretical studies on the spectral properties of frequency-nondegenerate type-I SPDC. In the case of cw-pumping, the two-photon joint spectral intensity function was found to be symmetric even though each photon had a different wavelength. We have shown that this is due to the fact that the joint spectral intensity function is forced to be symmetric by the narrow-band pumping condition even though the phase matching function itself is asymmetric. We have also demonstrated that the cw-pumped frequency-nondegenerate type-I SPDC exhibits a triangular single-photon interference envelope, which indicates that the spectral properties of SPDC photons are dependent on the first order of the detuning frequency as in the case of cw-pumped type-II SPDC.

For broadband pumping, the photon pair was found to have asymmetric joint spectral intensity function, different from the cw-pumped frequency-nondegenerate type-I SPDC but similar to the ultrafast-pumped type-II SPDC. Note that frequency-degenerate type-I SPDC does not exhibit the kind of pumping bandwidth-dependent behavior of the joint spectral intensity function.

Our study thus shows that frequency-nondegenerate type-I SPDC has spectral properties similar to those of type-II SPDC. We believe that the spectral studies reported here are expected to play important roles in developing ultrabright engineered two-color entangled photon sources.

ACKNOWLEDGMENTS

This work was supported by the Korea Research Foundation (Contract No. KRF-2006-312-C00551), the Korea Science and Engineering Foundation (Contact No. R01-2006-000-10354-0), and the Ministry of Knowledge and Economy of Korea through the Ultrashort Quantum Beam Facility Program.

[1] D. N. Klyshko, *Photons and Nonlinear Optics* (Gordon and Breach, New York, 1988).
[2] C. K. Hong and L. Mandel, Phys. Rev. Lett. **56**, 58 (1986).
[3] C. K. Hong, Z. Y. Ou, and L. Mandel, Phys. Rev. Lett. **59**, 2044 (1987).
[4] X. Y. Zou, L. J. Wang, and L. Mandel, Phys. Rev. Lett. **67**, 318 (1991).
[5] Y.-H. Kim, M. V. Chekhova, S. P. Kulik, Y. H. Shih, and M. H. Rubin, Phys. Rev. A **61**, 051803(R) (2000).
[6] J. G. Rarity, P. R. Tapster, E. Jakeman, T. Larchuk, R. A. Campos, M. C. Teich, and B. E. A. Saleh, Phys. Rev. Lett. **65**, 1348 (1990).
[7] Y. H. Shih and C. O. Alley, Phys. Rev. Lett. **61**, 2921 (1988).
[8] Y.-H. Kim, R. Yu, S. P. Kulik, Y. H. Shih, and M. O. Scully, Phys. Rev. Lett. **84**, 1 (2000).
[9] W. T. M. Irvine, J. F. Hodelin, C. Simon, and D. Bouwmeester, Phys. Rev. Lett. **95**, 030401 (2005).
[10] P. G. Kwiat, K. Mattle, H. Weinfurter, A. Zeilinger, A. V. Sergienko, and Y. H. Shih, Phys. Rev. Lett. **75**, 4337 (1995).
[11] P. G. Kwiat, E. Waks, A. G. White, I. Appelbaum, and P. H. Eberhard, Phys. Rev. A **60**, R773 (1999).
[12] Y.-H. Kim, S. P. Kulik, M. V. Chekhova, W. P. Grice, and Y. H. Shih, Phys. Rev. A **67**, 010301(R) (2003).
[13] Y.-H. Kim, Phys. Rev. A **68**, 013804 (2003).
[14] A. Fedrizzi, T. Herbst, A. Poppe, T. Jennewein, and A. Zeilinger, Opt. Express **15**, 15377 (2007).
[15] C. Cinelli, G. Di Nepi, F. De Martini, M. Barbieri, and P. Mataloni, Phys. Rev. A **70**, 022321 (2004).
[16] G. Vallone, E. Pomarico, F. De Martini, P. Mataloni, and M. Barbieri, Phys. Rev. A **76**, 012319 (2007).
[17] R. T. Thew, A. Acín, H. Zbinden, and N. Gisin, Phys. Rev. Lett. **93**, 010503 (2004).
[18] J. Brendel, E. Mohler, and W. Martienssen, Phys. Rev. Lett. **66**, 1142 (1991).
[19] P. G. Kwiat, A. M. Steinberg, and R. Y. Chiao, Phys. Rev. A **47**, R2472 (1993).
[20] D. V. Strekalov, T. B. Pittman, A. V. Sergienko, Y. H. Shih, and P. G. Kwiat, Phys. Rev. A **54**, R1 (1996).
[21] J. Brendel, N. Gisin, W. Tittel, and H. Zbinden, Phys. Rev. Lett. **82**, 2594 (1999).
[22] A. Rossi, G. Vallone, F. De Martini, and P. Mataloni, Phys. Rev. A **78**, 012345 (2008).
[23] T. B. Pittman, D. V. Strekalov, D. N. Klyshko, M. H. Rubin, A. V. Sergienko, and Y. H. Shih, Phys. Rev. A **53**, 2804 (1996).
[24] D. V. Strekalov, A. V. Sergienko, D. N. Klyshko, and Y. H. Shih, Phys. Rev. Lett. **74**, 3600 (1995).
[25] M. D'Angelo, Y.-H. Kim, S. P. Kulik, and Y. H. Shih, Phys. Rev. Lett. **92**, 233601 (2004).
[26] M. N. O'Sullivan-Hale, I. A. Khan, R. W. Boyd, and J. C. Howell, Phys. Rev. Lett. **94**, 220501 (2005).
[27] L. Neves, G. Lima, J. G. Aguirre Gómez, C. H. Monken, C. Saavedra, and S. Pádua, Phys. Rev. Lett. **94**, 100501 (2005).

[28] P. Walther, J.-W. Pan, M. Aspelmeyer, R. Ursin, S. Gasparoni, and A. Zeilinger, Nature (London) **429**, 158 (2004).
[29] M. Mitchell, J. Lundeen, and A. Steinberg, Nature (London) **429**, 161 (2004).
[30] A. Mair, A. Vaziri, G. Weihs, and A. Zeilinger, Nature (London) **412**, 313 (2001).
[31] A. Vaziri, G. Weihs, and A. Zeilinger, Phys. Rev. Lett. **89**, 240401 (2002).
[32] N. K. Langford, R. B. Dalton, M. D. Harvey, J. L. O'Brien, G. J. Pryde, A. Gilchrist, S. D. Bartlett, and A. G. White, Phys. Rev. Lett. **93**, 053601 (2004).
[33] J. G. Rarity and P. R. Tapster, Phys. Rev. Lett. **64**, 2495 (1990).
[34] Y.-H. Kim, S. P. Kulik, and Y. H. Shih, Phys. Rev. A **62**, 011802(R) (2000).
[35] J. T. Barreiro, T.-C. Wei, and P. G. Kwiat, Nat. Phys. **4**, 282 (2008).
[36] M. Barbieri, C. Cinelli, P. Mataloni, and F. De Martini, Phys. Rev. A **72**, 052110 (2005).
[37] M. Barbieri, G. Vallone, P. Mataloni, and F. De Martini, Phys. Rev. A **75**, 042317 (2007).
[38] A. Rossi, G. Vallone, A. Chiuri, F. De Martini, and P. Mataloni, Phys. Rev. Lett. **102**, 153902 (2009).
[39] M. V. Fedorov, M. A. Efremov, A. E. Kazakov, K. W. Chan, C. K. Law, and J. H. Eberly, Phys. Rev. A **69**, 052117 (2004).
[40] M. V. Fedorov, M. A. Efremov, A. E. Kazakov, K. W. Chan, C. K. Law, and J. H. Eberly, Phys. Rev. A **72**, 032110 (2005).
[41] M. V. Fedorov, M. A. Efremov, P. A. Volkov, E. V. Moreva, S. S. Straupe, and S. P. Kulik, Phys. Rev. Lett. **99**, 063901 (2007).
[42] Y.-H. Kim and W. P. Grice, J. Mod. Opt. **49**, 2309 (2002).
[43] Y.-H. Kim and W. P. Grice, Opt. Lett. **30**, 908 (2005).
[44] H. S. Poh, C. Y. Lum, I. Marcikic, A. Lamas-Linares, and C. Kurtsiefer, Phys. Rev. A **75**, 043816 (2007).
[45] W. Wasilewski, P. Wasylczyk, P. Kolenderski, K. Banaszek, and C. Radzewicz, Opt. Lett. **31**, 1130 (2006).
[46] A. V. Sergienko, Y. H. Shih, and M. H. Rubin, J. Opt. Soc. Am. B **12**, 859 (1995).
[47] D. V. Strekalov, Y.-H. Kim, and Y. H. Shih, Phys. Rev. A **60**, 2685 (1999).
[48] Y.-H. Kim, J. Opt. Soc. Am. B **20**, 1959 (2003).
[49] S.-Y. Baek and Y.-H. Kim, Phys. Rev. A **77**, 043807 (2008).
[50] Y.-H. Kim, S. P. Kulik, and Y. H. Shih, Phys. Rev. Lett. **86**, 1370 (2001).
[51] I. Marcikic, H. de Ridmatten, W. Tittel, H. Zbinden, and N. Gisin, Nature (London) **421**, 509 (2003).
[52] H. de Riedmatten, I. Marcikic, V. Scarani, W. Tittel, H. Zbinden, and N. Gisin, Phys. Rev. A **69**, 050304(R) (2004).
[53] S.-Y. Baek and Y.-H. Kim, Phys. Rev. A **75**, 034309 (2007).
[54] S.-Y. Baek and Y.-H. Kim, Phys. Lett. A **370**, 28 (2007).
[55] S.-Y. Baek, S. S. Straupe, A. P. Shurupov, S. P. Kulik, and Y.-H. Kim, Phys. Rev. A **78**, 042321 (2008).
[56] X.-H. Bao, Y. Qian, J. Yang, H. Zhang, Z.-B. Chen, T. Yang, and J.-W. Pan, Phys. Rev. Lett. **101**, 190501 (2008).
[57] H. Takesue, Phys. Rev. Lett. **101**, 173901 (2008).
[58] M. H. Rubin and Y. H. Shih, Phys. Rev. A **78**, 033836 (2008).
[59] S.-H. Tan, B. I. Erkmen, V. Giovannetti, S. Guha, S. Lloyd, L. Maccone, S. Pirandola, and J. H. Shapiro, Phys. Rev. Lett. **101**, 253601 (2008).
[60] W. P. Grice and I. A. Walmsley, Phys. Rev. A **56**, 1627 (1997).